ELSEVIER

Electrical Power and Energy Systems 26 (2004) 381–388

ELECTRICAL POWER & ENERGY SYSTEMS

www.elsevier.com/locate/ijepes

# Modeling and simulation of SVC and TCSC to study their limits on maximum loadability point

A. Kazemi[a], B. Badrzadeh[b,*]

[a]Department of Electrical Engineering, Iran University of Science and Technology, Tehran, Iran
[b]School of Engineering, The Robert Gordon University, AB10 1FR Aberdeen, UK

Received 14 December 2002; revised 3 October 2003; accepted 7 November 2003

**Abstract**

This paper presents the steady state modeling of static var compensator (SVC) and thyristor controlled series capacitor (TCSC) with their control and limits. Handling of limits and control mode switching are presented and discussed. Bifurcation analysis is applied in order to find the optimal location and rating of these devices and a continuation power flow is used to evaluate the effects of these devices on system loadability. Eigenvector analysis applied at the maximum loading point is used to rank the most critical voltage buses. After that, it would be possible to optimize location, sizing and control modes of SVC and TCSC in order to achieve maximum enhancement of system loadability. The models and methodology for placing and designing SVC and TCSC are tested in a 173 bus AC/DC system. Performance factors are defined to evaluate the efficiency of SVC and TCSC on different conditions.


*Keywords:* FACTS; SVC; TCSC; Static voltage collapse; Bifurcation; Maximum loadability point

## 1. Introduction

The phenomena of voltage collapse have been observed in power systems and analyzed extensively during the two past decades. Although major incidents were relatively rare, the seriousness of their consequences presented enough motivation for many researchers. Voltage collapse cases were reported in France, Italy, Japan, Great Britain, WSCC in USA… [1,2].

One simple method to find maximum loadability limit is to use an ordinary power flow and to gradually increase loads until convergence is no longer obtained [3]. In addition to the need for manual intervention, this approach often suffers from convergence and one is never certain where the limits actually are. A more precise determination of the proximity of a limit is essential when one is interested in effects of various possible control actions on the location of these limits. In addition, the conventional power flow method is generally not able to reliably find low voltage solutions that are necessary for some of the direct energy function methods etc. This paper uses continuation power flow method [3,4] for determining of point of collapse or maximum loadability point.

Voltage collapse typically occurs on power systems that are heavily loaded, faulted and/or have reactive power shortage. Voltage collapse is a system instability in that it involves many power system components and their variable at once. Indeed, voltage collapse often involves an entire power system, although it usually has a relatively larger involvement in one particular area of the power system [3].

Although many other variables are typically involved, some physical insight into the nature of voltage collapse may be gained by examining the production, transmission and consumption of reactive power. Voltage collapse is associated with the reactive power demands of loads not being met because of limitations on the production and transmission of reactive power. Limitations on the production of reactive power include generator and FACTS reactive power limits and the reduced reactive power produced by capacitors at low voltages [3]. The primary limitations on the transmission of reactive power are high reactive power loss on heavily loaded lines and line outages. Reactive power demands of loads increase with load

* Corresponding author.
*E-mail address:* prs.badrzadeh@rgu.ac.uk (B. Badrzadeh).

0142-0615/$ - see front matter © 2003 Elsevier Ltd. All rights reserved.
doi:10.1016/j.ijepes.2003.11.007

increases, motor stalling, or change in load composition such as an increased proportion of compressor load.

This paper concentrates on static voltage collapse that means voltage; active power and reactive power flow problems have been analyzed using static power flow programs [3]. This approach was satisfactory since these problems have been governed by essentially static or time independent factors. Power flow analysis allows simulation of a snapshot of time, such as after automatic actions but before operator actions. Static analysis involves only the solution of algebraic equations and therefore is computationally much more efficient than dynamic analysis. Static analysis is ideal for the bulk of studies in which voltage stability limits for many pre-contingency and post-contingency cases must be determined [3].

Conventional power systems usually are controlled mechanically. With mechanical devices such as circuit breakers, control cannot be initiated frequently because mechanical devices tend to wear out quickly compared to static devices. The central technology of FACTS involves high power electronics, a variety of thyristor devices, microelectronics, communications and advanced control centers. Power flow through an AC line is a function of phase angle, line end voltages and line impedance and there is little or no control over any of these variables. The consequences of this lack of fast, reliable control are stability problems, power flowing through other than the intended lines, the inability to fully utilize the transmission resources, undesirable var flows, higher losses, high or low voltage, cascade tripping and long restoration times. With FACTS devices one can control the phase angle, the voltage magnitude at chosen buses and/or line impedances. Power flow is electronically controlled and it flows as ordered by control center.

In Ref. [5], an approximate model of static var compensator (SVC) is used for the computations. In Ref. [6], steady state model of SVC and thyristor controlled series capacitor (TCSC), including control and limits are proposed. The authors also present a method for placing and designing SVCs and TCSCs, within a system, such that its loadability margin is increased in a most efficient way. The results are presented on 14 bus AC/DC system. The present paper uses a similar method of Ref. [6], but the utilized model [7,8,9] is more general than Ref. [6], so that it can be used for both power flow and transient stability based programs. This model is validated using a large AC/DC system (173 bus).

## 2. Saddle node bifurcation

The typical quasi-steady-state description of a power system, corresponding to a transient stability model, is given by the differential-algebraic equations [3]:

$$x' = f(x, y, \lambda, p) \tag{1}$$

$$0 = g(x, y, \lambda, p)$$

Where $x$ corresponds to the system state variables, and $y$ represents the algebraic variables. The variable $\lambda$ stands for a parameter or a set of parameters that slowly change in time, so that the system moves from one equilibrium point to another until reaching the collapse point and $p$ stands for a parameter that is directly controllable, such as shunt and series compensations. (The value of $\lambda$ at equilibrium point ($\lambda_o$) corresponds to the maximum loading level or loadability margin in p.u.)

It is shown that static voltage collapse can be studied using saddle node bifurcation (related to zero eigenvalues) [4]; a saddle node bifurcation is the disappearance of system equilibrium as parameters change slowly [3]. The assumption of slow parameter variation means that the parameters vary slowly with respect to the system dynamics. For example, before bifurcation when the system state is tracking the stable equilibrium, the system dynamics act more quickly to restore the operating equilibrium than the parameter variations do to change the operating equilibrium. The saddle node bifurcation of most interest to power system engineers occurs when a stable equilibrium at which the power system operates disappears. The consequence of this loss of the operating equilibrium is that system states change dynamically. In particular, the dynamics can be such that the system voltages fall into a voltage collapse.

Saddle node bifurcation is an inherently nonlinear phenomena and it cannot occur in a linear model. However, the phenomena of saddle node bifurcation is familiar from as simple a nonlinear model as a quadratic equation [3]. If the quadratic equation has two real roots (equilibrium points), as the coefficients (parameters) of a quadratic equation change slowly, the two real roots move and it is possible and routine for real roots to disappear. The bifurcation occurs at the critical case of a double root that separates the case of two real roots from the case of no real roots.

If the system Jacobin is asymptotically stable (the usual case), all eigenvalues have negative real parts. What happens, as loading increases slowly to the critical loading is that one of the Jacobin eigenvalues approaches zero from the left. The main use of the Jacobin is that it determines the stability of the system linearized about an equilibrium.

## 3. SVC model

The basic structure of an SVC operating under typical bus voltage control is depicted in the block diagram of Fig. 1 [6]. Each phase of this FACTS controller is typically made up of a thyristor-controlled reactor (TCR) in parallel with a fixed capacitor bank (FC); the system is then shunt connected to the bus through a step-up transformer bank to bring the voltages up to the required transmission levels. (This transformer will be treated similarly to the other transformers in the system). By controlling the firing angle $\alpha$ of the thyristors (the angle with respect to zero-crossing of

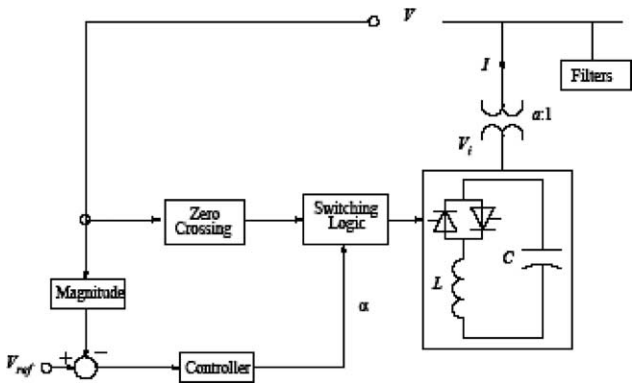


Fig. 1. Block diagram of a SVC with voltage control.

the phase voltage), the device is able to control the bus voltage magnitude, as changes on $\alpha$ basically result on changes in the current and, hence, the amount of reactive power consumed by the inductor $L$; for $\alpha = 90°$ the inductor is fully on, whereas for $\alpha = 180°$ the inductor is off. The continuous switching operations of the TCR generate certain harmonic pollution on the voltage waveforms that have to be taken into account for the design and operation of the controller.

The basic control strategy is typically to keep the transmission bus voltage within certain narrow limits defined by a controller droop and the firing angle $\alpha$ limits ($90° < \alpha < 180°$).

Assuming balanced, fundamental frequency operation, an adequate transient stability model can be developed assuming sinusoidal voltages. This model can be represented by the following set of p.u. equations [7,8]:

$$[x_c{}', \alpha']^T = f(x_c, \alpha, V, V_{REF}) \tag{2}$$

$$B_e - (2\alpha - \sin\alpha - \pi(2 - X_L/X_C))/\pi X_L = 0$$

$$I_{SVC} - V_i B_e = 0$$

$$Q_{SVC} - V_i^2 = 0$$

Where $f(\cdot)$ stands for the control system variables and equations, respectively; $V$ stands for the controlled bus voltage magnitude; $V_i$ represents the TCR and fixed

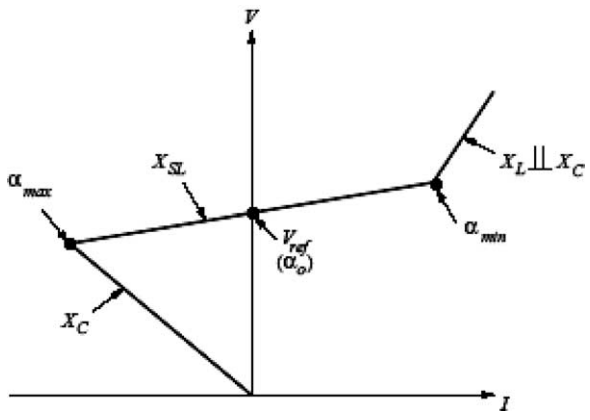


Fig. 2. Typical steady state $V$–$I$ characteristic of a SVC.

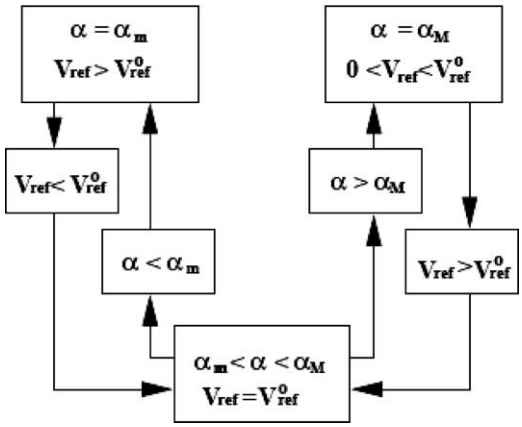


Fig. 3. Handling of limits in the SVC steady state model.

capacitor voltage magnitude; $V_{REF}$ is the controller set point and $X_{SL}$ stands for droop; $Q_{SVC}$ and $I_{SVC}$ are the controller reactive power and current, respectively; $B_e$ is the equivalent suseptance of the TCR and fixed capacitor combination and $X_C$ and $X_L$ correspond to the fundamental frequency reactance of $L$ and $C$, respectively. The steady state $V$–$I$ characteristics of this controller are depicted in Fig. 2, and correspond to the well-known control characteristics of a typical SVC. A SVC steady state model can be obtained by replacing the differential equations in (2) with the corresponding equations representing the steady state characteristics; thus, the power flow equations of the SVC in this case are [7,8]:

$$V - V_{REF} + X_{SL} I = 0 \tag{3}$$

$$B_e - (2\alpha - \sin\alpha - \pi(2 - X_L/X_C))/\pi X_L = 0$$

$$I_{SVC} - V_i B_e = 0$$

$$Q_{SVC} - V_i^2 = 0$$

Which can be included in any power flow program, however, for the model to be complete, all SVC controller limits should be adequately represented (Fig. 3). SVC limits are considered as firing angle $\alpha$; i.e. $\alpha \in [\alpha_m, \alpha_M]$; where $\alpha_m$ is the minimum firing angle and $\alpha_M$ is the maximum firing angle. Fig. 3 shows handling of firing limits for SVC, where $V_{REF}$ is fixed at $V_{REF}^o$, until $\alpha$ reaches a limit, at which point $V_{REF}$ is allowed to change while $\alpha$ is kept at its limit value; voltage control is regained when $V_{REF}$ returns to $V_{REF}^o$ [8].

## 4. TCSC model

Fig. 4 shows the block diagram for a TCSC controller operating under current control. This FACTS controller basically consists of the same TCR and FC combination used in SVC but connected in series with a transmission line. Due to series connection, there is no need in this case for a transformer bank to change the controller voltage. This device is usually designed to directly control line currents,

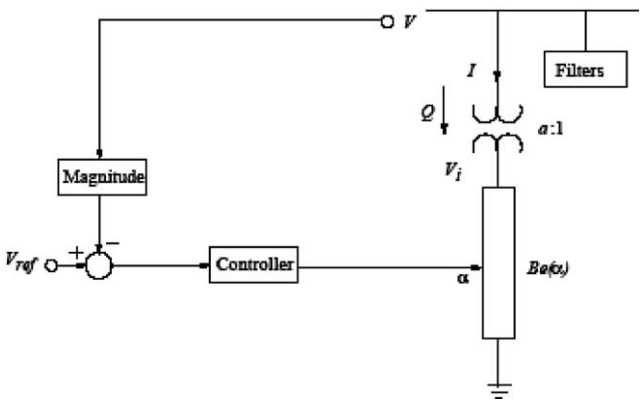


Fig. 4. Block diagram of a TCSC operating in current control mode.

but various other strategies can be used to control line impedance and power flows, damp oscillations, etc.

The limits on the firing angle $\alpha$ for the TCSC controller are different from the ones used for the SVC, as there is a resonance region where the controller becomes an open circuit and, hence, it must be avoided in a series connection. Furthermore, the controller is designed to mainly operate in the capacitive region in steady state, to reduce harmonic pollution of the current waveforms. Thus, for this paper $\alpha_r < \alpha < 180°$, where $\alpha_r$ corresponds to the resonant point (this value depends on the ratio $X_C/X_L$).

Fundamental frequency operation can be represented by the following set of equations, which includes the control system equations and assumes sinusoidal currents in the controller [7,8]:

$$[x_c', \alpha']^T = f(x_c, \alpha, I, I_{REF}) \tag{4}$$

$$P + V_k V_m B_e \sin(\delta_k - \delta_m) = 0$$

$$-V_k^2 B_e + V_k V_m B_e \cos(\delta_k - \delta_m) - Q_k = 0$$

$$-V_m^2 B_e + V_k V_m B_e \cos(\delta_k - \delta_m) - Q_m = 0$$

$$B_e - B_e(\alpha) = 0$$

$$(P^2 + Q_k^2)^{1/2} - IV_k = 0$$

Where $x_c$ and $f(\cdot)$ stand for the internal control system variables and equations; $V_k$ and $V_m$ are the magnitudes of terminal voltages of controller; $\delta_k$ and $\delta_m$ are the phases of the terminal voltages of the controller; $Q_k$ and $Q_m$ are the reactive power injections at both controller terminals; $P$ and $I$ are the active power and current flowing through the controller, respectively, the values of $B_e$, $X_C$ and $X_L$ are explained in Section 3 and $B_e(\alpha)$[7,8]:

$$\begin{aligned} B_e(\alpha) = {} & \pi(k_x^4 - 2k_x^2 + 1)\cos k_x(\pi - \alpha)/[X_c(\pi k_x^4 \cos k_x(\pi - \alpha) \\ & - \pi \cos(k_x - \alpha) - 2k_x^4 \alpha \cos k_x(\pi - \alpha) \\ & + 2\alpha k_x^2 \cos k_x(\pi - \alpha) - k_x^4 \sin 2\alpha \cos k_x(\pi - \alpha) \\ & + k_x^2 \sin 2\alpha \cos k_x(\pi - \alpha) - 4k_x^3 \cos^2 \alpha \sin k_x(\pi - \alpha) \\ & - 4k_x^2 \cos \alpha \sin \alpha \cos k_x(\pi - \alpha) \end{aligned} \tag{5}$$

where $k_x = (X_C/X_L)^{1/2}$.

It is important to mention that as the controller gets closer to its resonant point, the current deviates from its sinusoidal condition, and hence the model presented should not be used to represent the controller under these conditions [9].

A steady state model for this TCSC controller can be obtained by replacing the differential equations on (5) with the corresponding steady state control equations. For example, for an impedance control model with no droop, which yields the simplest set of steady state equations from the numerical point of view, the power flow equations for the TCSC are [7,8]:

$$B_e - B_{REF} = 0 \tag{6}$$

$$P + V_k V_m B_e \sin(\delta_k - \delta_m) = 0$$

$$-V_k^2 B_e + V_k V_m B_e \cos(\delta_k - \delta_m) - Q_k = 0$$

$$B_e - B_e(\alpha) = 0$$

$$(P^2 + Q_k^2)^{1/2} - IV_k = 0$$

The TCSC control limits are basically limits on the firing angle $\alpha$. If $\alpha$ hits a limit the firing angle fixed at corresponding limit and control limit is switched to reactance control ($B_e - B_{REF} = 0$).

## 5. Continuation power flow

Continuation methods overcome certain difficulties of successive power flow solution methods, as they are not based on a particular system model, and allow the user to trace the complete voltage profile by automatically changing the value of λ, without having to worry about singularities of system equations. The strategy used in these methods is shown in Fig. 5 [3], where a known equilibrium point $(z_1, \lambda_1)$ is used to compute the direction vector $\Delta z_1$ and a change $\Delta\lambda_1$ of the system parameter. This first step is known as the predictor, since it generates an initial guess $(z_1 + \Delta z_1, \lambda_1 + \Delta\lambda_1)$, which is then used in the corrector step to compute a new equilibrium point $(z_2, \lambda_2)$ on the system profile. Since the Jacobin $D_z F|^*$ is singular at the collapse point, a parameterization is sometimes needed in the predictor and/or corrector steps, depending on the techniques used, to guarantee a well behaved numerical solution of the related equations.

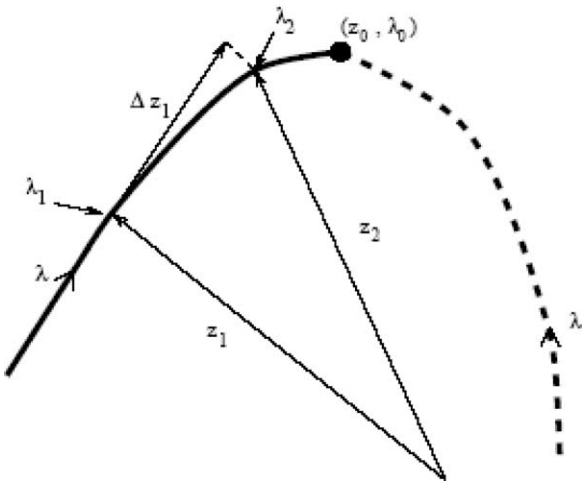


Fig. 5. Continuation method.

A detailed description of these techniques is referred to Refs. [10–11].

## 6. Test system

Fig. 6 shows the one-line diagram corresponding to the 173 bus AC/DC system used in this paper [12]. This system is a simplified version of a real 2158 bus network with AC transmission voltage levels of 500 kV. It was developed as a part of EPRI project. Both rectifier stations are weakly coupled through a 500 kV transmission system where as the inverter ends are tightly coupled through a 500–345–230 kV AC network. The DC link on the left of Fig. 6 is a 12 pulse bipolar HVDC system with a positive or negative 500 kV DC voltage level and 3000 MW capacity; the second HVDC system is also a 12 pulse bipolar DC linked designed for 500 kV and 2000 MW nominal levels. The AC system has 29 generators, 203 transmission lines and transformers, and 52 series capacitors. Typical $V$ and $Q$, and tap limits for regulating transformers included.

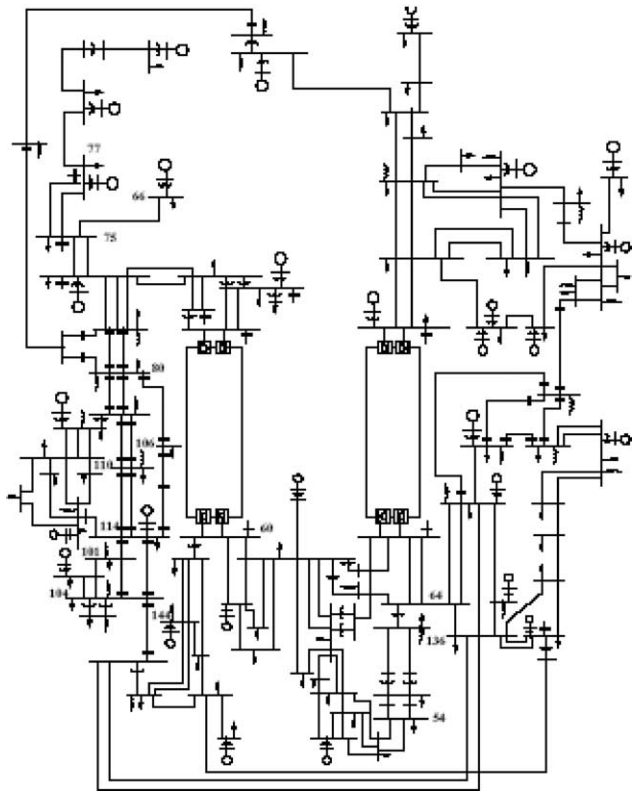

Fig. 6. 173 Bus AC/DC test system.

## 7. Results

The voltage profiles at chosen buses are shown in Fig. 7. These are the 4 voltages that change the most with respect to the loading of the system. The total active load for the base case is $P_{\text{total}} = 56,216.91$ MW. The active and reactive load is increased discretely, according to the load model. The PV diagrams are used to show the voltage profiles versus the total active load, since. Notice that the voltage profiles in the PV diagram are quite flat, which means that there is significant voltage support in the system. The bifurcation point is reached at high values of the voltages, close to 1.0 p.u., Which indicates that the voltages itself is a poor indicator of voltage collapse.

Eigenvector analysis applied at the bifurcation point provided the buses that lack voltage support the most at the buses 114, 101 and 75. To design the SVC, bus 114 was changed into a PV bus with the voltage fixed at 0.98 p.u. The solution to the power flow at the loading level where the original system bifurcates, i.e. $P_{\text{total}}^{\text{bif}} = 57,656.06$ MW indicates that the required reactive power injection is about 200 MVar. The inductive rating of the SVC is assumed to the equal to its capacitive rating; therefore, $Q_{SVC} = 200$ MVar. The slope of the SVC is 2%. The bifurcation diagram for the SVC placed at bus 114 is

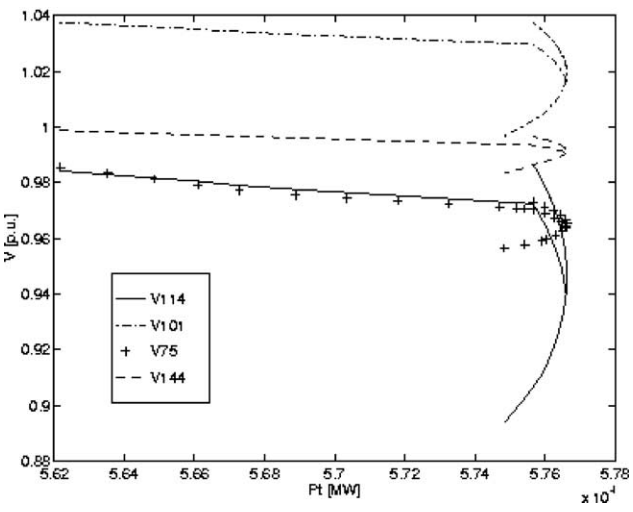


Fig. 7. Voltage profile for 173 bus AC/DC System without FACTS.

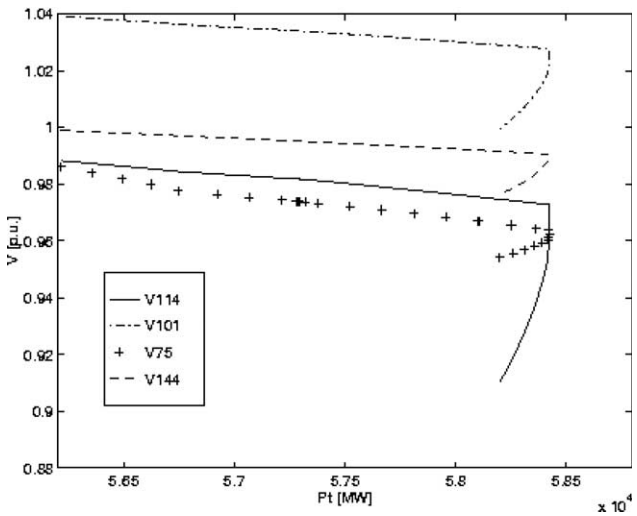


Fig. 8. Voltage profiles for 173 bus AC/DC system with $Q_{SVC} = 200$ MVar, slope 2%, $V_{REF} = 1.0$ at bus 114.

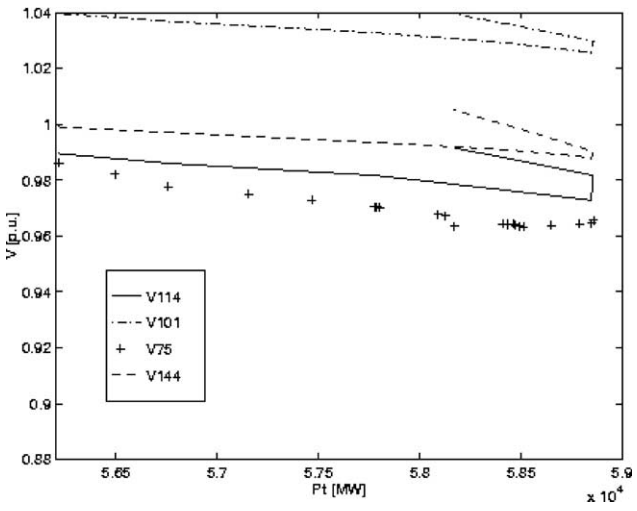


Fig. 9. Voltage profiles for 173 bus AC/DC system with $Q_{SVC} = 300$ MVar, slope = 2%, $V_{REF} = 1.0$ at bus 114.

presented in Fig. 8. The bifurcation occurs at $P^{bif}_{total} = 58,431.86$ MW, which is 3.94% more than the base load. The performance factor is $f_p = 11.075$ ($f_p = \lambda_o[MW]/Q_{SVC}[MVar]$). The system with the SVC placed at bus 114 is capable of delivering 2214.95 MW of additional power for a 200 MVar rating of the SVC. Table 1 compares the results for the same SVC placed at buses 101 and 75. As can be concluded, maximum loadability points are 0.85 and 1.12% less than the SVC placed at bus 114, respectively.

Bifurcation analysis is performed on the system with the SVC placed at bus 114. The analysis indicates that voltage support is again mostly needed at bus 114. The same design method as previously shown is used and the amount of additional reactive support is about 100 MVar; therefore, a SVC of rating $Q_{SVC} = 300$ MVar is placed at bus 114 replacing the 200 MVar SVC. The same transformer is used with a new rating equal to the new SVC rating. The voltage profiles are shown in Fig. 9. The maximum load is now $P^{bif}_{total} = 58,856.29$ MW or 0.72% more than for the 200 MVar SVC at the same bus. It can be concluded that this improvement is marginal with respect to the base case, where the 200 MVar SVC was placed at bus 114. For the 200 MVar SVC placed at bus 114 the performance factor is $f_{p1} = 11.075$, whereas for the 300 MVar SVC placed at the same bus the new performance factor is $f_{p2} = 8.798$, which is considerably lower. In other words, placing the 200 MVar SVC at bus 114 is more cost effective than placing an additional 100 MVar at that bus by rating the SVC at 300 MVar. Another location is chosen at bus 60 for a second SVC rated at 100 MVar. This corresponds to the extra 100 MVar added to the SVC at bus 114. The voltage reference is set at 1.0 p.u. due to the initial voltage profile at bus 60. Fig. 10 presents the results for this 2 SVC case. The maximum load is $P^{bif}_{total} = 58,437.47$ MW or 0.01% higher than for the 200 MVar SVC placed at bus 114.

Table 1
Effect of SVC sizing and location on the loadability margin of the system

| SVC location | SVC size (MVar) | Percentage of improvement to base case | Performance factor |
|---|---|---|---|
| Bus 114 | 200 | 3.94 | 11.075 |
| Bus 101 | 200 | 3.09 | 8.698 |
| Bus 75 | 200 | 2.82 | 7.926 |
| Bus 114 | 300 | 4.66 | 8.978 |
| Bus 114 + Bus 60 | 200 + 100 | 3.95 | 7.401 |

Table 1 depicts the impact of SVC sizing and location on loadability margin of the system.

Eigenvector analysis performed on the original system indicates that there is a lack of active support at buses 65,66, in that order, and 77,75 with a lower priority. For the system configuration with fixed generation, power flow through lines 66–75, 77–75 is fixed and cannot be

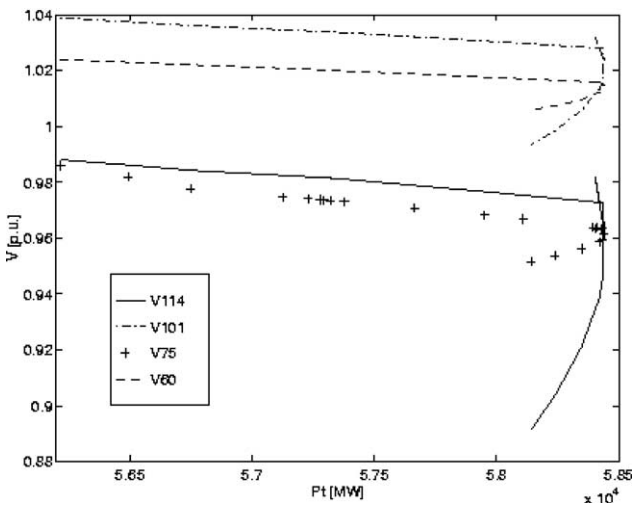


Fig. 10. Voltage profiles for 173 bus AC/DC system with $Q_{SVC1} = 200 \times$ MVar, slope = 2%, $V_{REF} = 1.01$ at bus 114 and $Q_{SVC2} = 100$ MVar, slope = 2%, $V_{REF} = 1.02$ at bus.

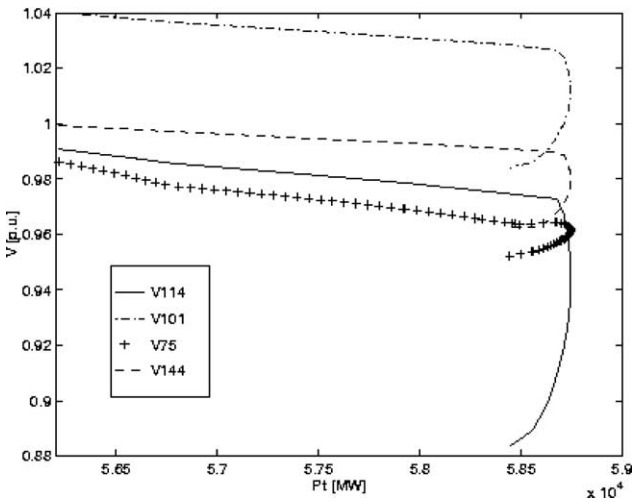


Fig. 11. Voltage profiles for 173 bus AC/DC system, TCSC on line 110–114 (short), 90% compensation.

affected by series compensation because there are no alternative routes for the power to flow. (Fig. 6). The next buses with lack of active support are buses 136,54 and 114. The most heavily loaded lines are lines 114–106,114–110 (short) and 114–110 (long), in that order. All of these lines are already series compensated. Bus 114 is connected to the bus110 through 2 lines, a short line and a long line. Fig. 11 shows the voltage profile for a TCSC placed on the line 114–110 (short), at bus 114. The control is reactance control with 90% compensation level. The maximum load in this case is $P_{\text{total}}^{\text{bif}} = 58,744.42$ MW or 4.5% higher than the base case. Fig. 12 shows the results for the same TCSC with power control fixed at the corresponding power flowing through the line at base loading and 90% compensation. The maximum load is $P_{\text{total}}^{\text{bif}} = 58,646.04$ MW or 4.3% higher than the base case. In Fig. 13, the voltage profiles are

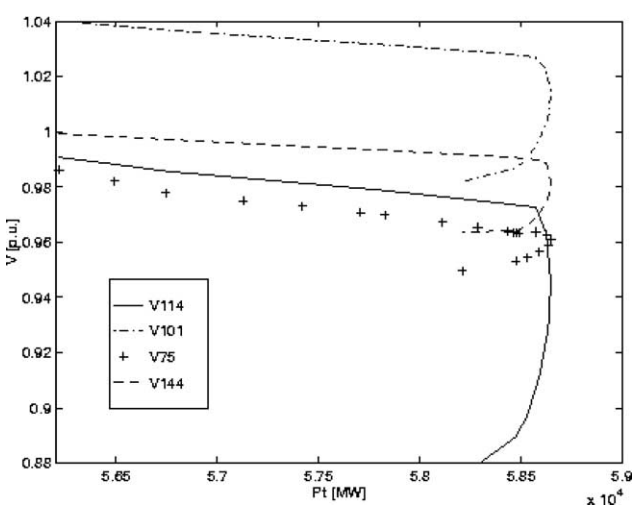


Fig. 12. Voltage profile for 173 bus AC/DC system, TCSC On line 114–110 (short) power control.

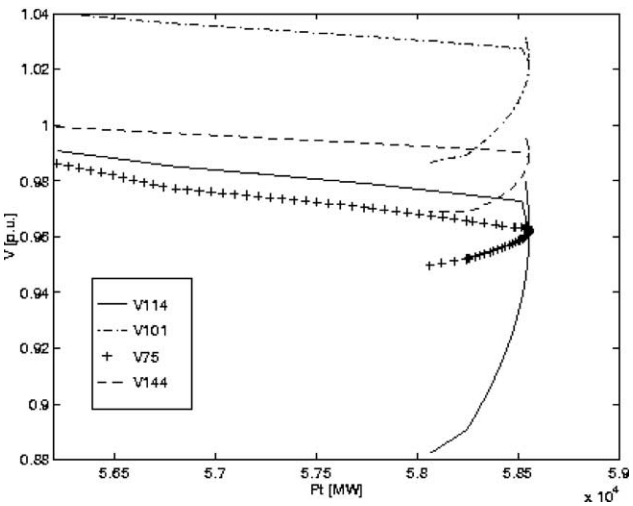


Fig. 13. Voltage profiles for 173 bus AC/DC system, TCSC on line 114–110 (short) current control.

presented for the same TCSC with current control set at the value of the current corresponding to base case loading and 90% line compensation. The maximum load is $P_{\text{total}}^{\text{bif}} = 58,555.53$ MW or 4.16% more than the base-case. In Fig. 14, the PV diagram is presented for constant transmission angle control, set at the angle corresponding to base loading and 90% line compensation. The maximum power is in this case $P_{\text{total}}^{\text{bif}} = 58,605.00$ MW or 4.25% higher than the base case. It is shown that the constant reactance control strategy provided the maximum loadability margin. Fig. 15 presents the results for a TCSC, placed on the line 114–110 (long), with constant reactance control, at 90% compensation level. The original compensation was 60%. The maximum load is $P_{\text{total}}^{\text{bif}} = 57,708.9$ MW or 2.65% increase with respect to the base case. Table 2 shows the effect of TCSC placement and control modes on the loadability margin of the system.

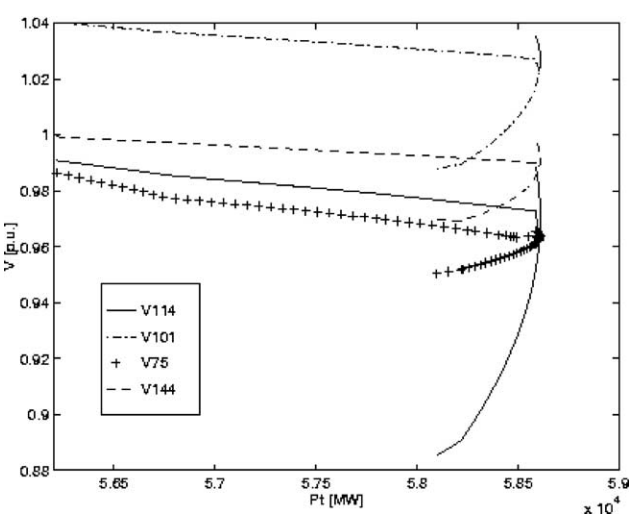


Fig. 14. Voltage profiles for 173 bus AC/DC system, TCSC on line 114–110 (short) transmission angle control.

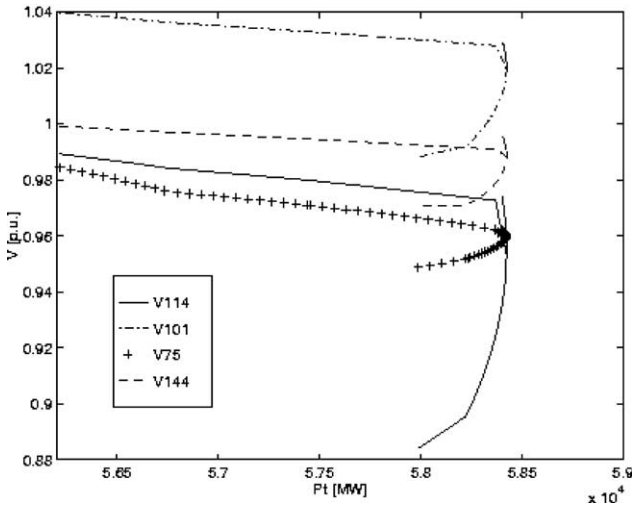


Fig. 15. Voltage profiles for 173 bus AC/DC system, TCSC on line 114–110 (long) with 90% compensation.

Table 2
Effect of TCSC placement and control modes on the loadability margin of the system

| TCSC location | Control modes | Percentage of improvement to base case |
|---|---|---|
| Line110–114 (short) | Reactance | 4.5 |
| Line110–114 (short) | Power | 4.3 |
| Line110–114 (short) | Current | 4.16 |
| Line110–114 (short) | Transmission angle | 4.25 |
| Line110–114 (long) | Reactance | 2.65 |

## 8. Conclusions

The transient stability and power flow models for SVC and TCSC are presented. These models cannot be reliably used to represent unbalanced system conditions, as they are all based on balanced voltage and current conditions. These models also are not adequate for large disturbances because of high harmonic content. Steady state (power flow) model includes control and limits of FACTS devices are proposed. Continuation power flow method is applied to implement these models in a power flow program. Finally, the most efficient way to increase maximum loadability point regarding location, size and control modes of FACTS is presented. Key achievement can be summarized as follows:

1. Voltage itself is a poor indicator of voltage collapse.
2. Even thouth placing a SVC with more capacity than optimum capacity at the most critical bus increase stability margin, it might lead to the reduction of performance factor.
3. Placing a single SVC at the most critical bus is more cost effective than placing extra SVCs at the other critical buses.
4. Even though all the said control strategies of TCSCs increase loadability margin of the system, Constant reactance control provided the most loadability margin.

## References

[1] Taylor CW. Power system voltage stability. New York: McGraw-Hill; 1994.
[2] Mansour Y. editor. Suggested techniques for voltage stability analysis. Technical Report 93TH0620-5PWR,IEEE/PES; 1993.
[3] Power system stability subcommittee report on voltage stability assessment, procedures and guides. IEEE/PES, Final draft; 1999.
[4] Canizares CA, Alvardo FL. Point of collapse method applied to large AC/DC system. IEEE Trans Power Syst 1993;8(1):1–8.
[5] Mansour Y, et al. SVC placement using critical modes of voltage instability. IEEE Trans Power Syst 1994;9(2):757–63.
[6] Canizares CA, Faur Z. Analysis of SVC and TCSC controllers in voltage collapse. IEEE Trans Power Syst 1999;14(1):1–8.
[7] Canizares CA. Modeling of TCR and VSI based FACTS controllers. Internal report ENEL and politechnico di milano, Milan; 1999.
[8] Canizares CA. et al. Using FACTS controllers to maximize available transfer capability. Bulk power systems and dynamics, part IV, restructing; 1998.
[9] Canizares CA. Power flow and transient stability models of FACTS controllers for voltage and angle stability studies. IEEE/PES WM panel on modeling, simulation and applications of FACTS devices; 2000.
[10] Huneault M, Galiana FD. An investigation of the solution to the optimal power flow problem incorporating continuation methods. IEEE Trans Power Syst 1990;5(1):103–10.
[11] Ajjarapu V, Christy C. The continuation power flow: a tool for steady state voltage stability analysis. IEEE Trans Power Syst 1992;7(2): 416–23.
[12] Methodology for integration of HVDC links in large AC systems. EPRI Technical Report EL-4365; 1987.